

Deep mutational scanning of hemagglutinin helps distinguish the evolutionary fate of human H3N2 influenza virus

Juhye M. Lee^{1,4,5,†}, John Huddleston^{2,6,†}, Michael B. Doud^{1,4,5},
Kathryn A. Hooper^{1,6}, Trevor Bedford^{2,3*} and
Jesse D. Bloom^{1,3,4*}

¹Basic Sciences Division, ²Vaccine and Infectious Diseases Division, and ³Computational Biology Program,
Fred Hutchinson Cancer Research Center, Seattle, WA, USA

⁴Department of Genome Sciences, ⁵Medical Scientist Training Program, and ⁶Molecular and Cellular Biology Program,
University of Washington, Seattle, WA, USA

[†]These authors contributed equally

*Correspondence: trevor@bedford.io, jbloom@fredhutch.org

Abstract

Abstract text.

INTRODUCTION

Very rough outline:

- Mutations are rampant in the evolution of human influenza virus. Seasonal H3N2 influenza virus in particular rapidly accumulates mutations.
- The evolution of H3N2 is also characterized by clade competition and population turnover.
- There have been efforts to predict evolutionary success.
- Mutations that contribute to antigenic evolution largely determine strain success.
- RNA viruses can accumulate deleterious mutations, and because the influenza does not appreciably recombine, deleterious mutations are linked to beneficial ones.
- Mutations in HA that impact viral growth may influence strain success.
- We need to understand the functional impact of mutations in HA.

- Previously, we measured the effect of all possible single amino-acid mutations to an H1 hemagglutinin from the A/WSN/1933 (H1N1) strain ([Thyagarajan and Bloom, 2014](#); [Doud and Bloom, 2016](#)).
- However, this is a highly lab-adapted strain, and the measurements in this strain may not be particularly relevant for studying mutational processes of more contemporaneous strains circulating in the human population.
- We chose to study the Perth/2009 H3 HA.
- This also enabled a comparison of how the preferences have shifted for two diverged HA's.

RESULTS

Deep mutational scanning of HA from a recent strain of human H3N2 influenza virus

We performed a deep mutational scan to measure the effects of all amino-acid mutations to the A/Perth/16/2009 (H3N2) HA on viral replication in cell culture. This strain was the H3N2 component of the influenza vaccine from 2010-2012. We used a variant of this HA that supported better viral replication in cell culture than did the sequence in GenBank (Figure S1). This HA variant contained two mutations: G78D and T212I. The G78D mutation occurs at low frequency in natural H3N2 sequences, and T212 is a site where a mutation to Ala rose to fixation in human influenza in ~2011.

We mutagenized the entire gene at the codon level to create mutant plasmid libraries harboring an average of ~1.4 codon mutations per clone. We then generated mutant virus libraries from the mutant plasmids using a helper virus system that enables the efficient generation of complex virus libraries ([Doud and Bloom, 2016](#)) (Figure 1A). In order to reduce biosafety concerns and to maximize viral titers, we used an HA-deficient helper virus carrying WSN/1933 internal and NA genes to rescue the mutant viruses. Additionally, we used MDCK-SIAT1 cells constitutively expressing the TMPRSS2 protease, which facilitates HA cleavage and activation in the human airway ([Böttcher et al., 2006](#); [Böttcher-Friebertshäuser, et al., 2010](#)). All of the experiments were completed in full biological triplicate (Figure 1B). We also passaged and deep sequenced library 3 in technical replicate (denoted as library 3-1 and 3-2) to gauge to the amount of experimental noise occurring *within* a single biological replicate. As a control, we used the unmutated gene to generate and passage viruses carrying wildtype HA.

Deep sequencing revealed selection against non-functional HA variants as evidenced by the reduced mutation frequencies of the mutant viruses compared to their starting frequencies in the mutant plasmids (Figure 1C). Specifically, stop codons were purged to 20-45% of their original starting frequencies, after correcting for error rates from the wildtype controls. Although the majority of stop codons were purged, incomplete purging of stop codons is likely due to complementation of virions. We also observed purging of nonsynonymous mutations to 30-40% of their initial starting frequencies after error correction, suggesting strong selection against deleterious HA variants.

We next quantified the reproducibility of our deep mutational scanning measurements across biological and technical replicates. We inferred the amino-acid preferences at each site in the Perth/2009 HA using the method described in Bloom (2015) and implemented in the dms_tools2 software [https://jbloomlab.github.io/dms_tools2/]. These preferences represent an estimate of the 567 sites \times 20 amino acids = 11340 experimental measurements and are normalized to sum to one at each site. The correlations of the amino-acid preferences between each pair of replicates is shown in Figure 1D. The biological replicates are fairly well-correlated, with a Pearson's R ranging from 0.69 to 0.78. Replicate 1 exhibits the least amount of correlation with the other biological replicates, consistent with the observation that this replicate showed the weakest selection against stop and nonsynonymous mutations and might therefore be subject to more experimental noise. Of note, the two technical replicates 3-1 and 3-2 were only slightly more reproducible than that between biological replicates. This suggests that bottlenecking of the virus library during the low MOI passage contributes to much of the noise observed in our experiments, as we are only able to passage a finite number of viral particles.

The HA preferences improve phylogenetic fit of natural H3 sequences

How well do the Perth/2009 HA preferences inferred from experimental measurements describe the evolution of H3N2 influenza virus in nature? This question can be addressed by evaluating how well experimentally informed codon substitution models (ExpCM's) constructed from our laboratory measurements improve phylogenetic fit of H3N2 evolution (Hilton et al., 2017). The results in Table 1 show that the ExpCM outperforms conventional substitution models in describing the evolution of human H3N2 HA. The ExpCM also optimizes a stringency parameter (β) for the preferences to more closely reflect the strength of selection in nature. The stringency parameter in the ExpCM is equal to 2.44, which indicates that although the same amino acids are preferred, the strength of selection is more stringent in nature than in our experiments. Figure 2 shows a logo plot of the Perth/2009 HA amino-acid preferences rescaled by this stringency parameter.

A closer examination of the logo plot reveals that the preferences generally agree with

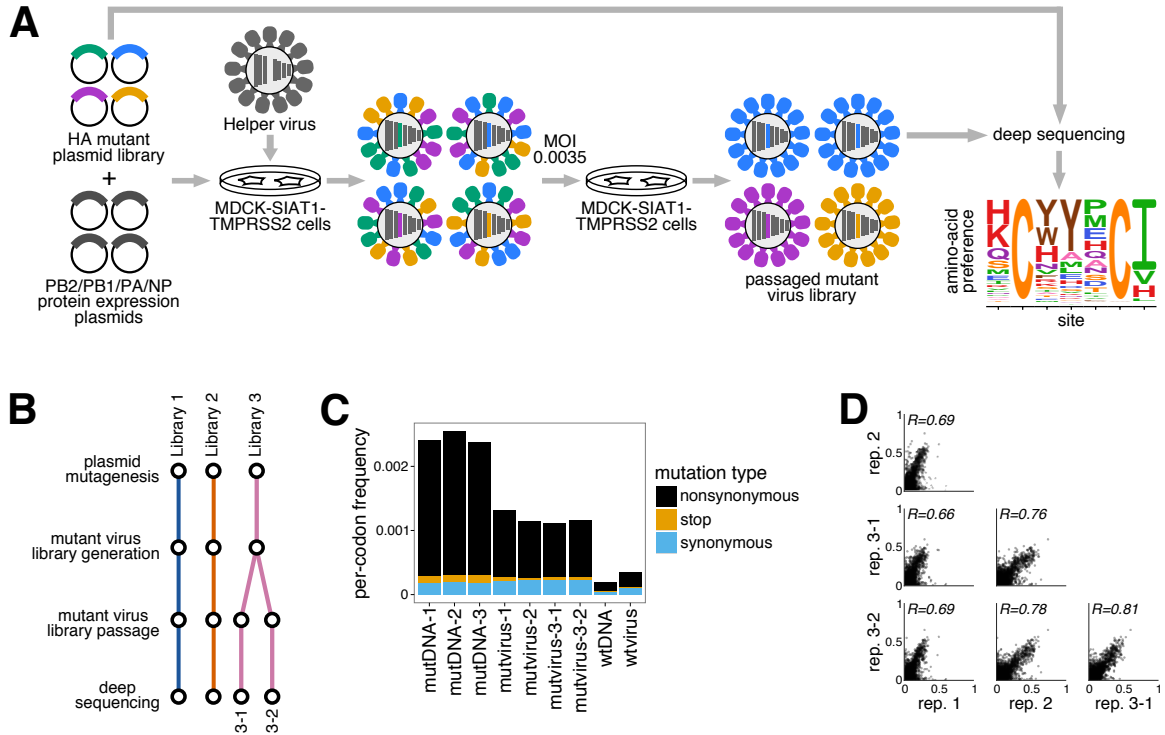


Figure 1: Deep mutational scanning experiments of H3 HA. (A) We generated Perth/2009 HA mutant virus libraries in MDCK-SIAT1-TMPRSS2 cells using a helper virus approach described in [Doud and Bloom \(2016\)](#). We then passed the initially generated pool of mutant viruses at low MOI to establish a genotype-phenotype linkage and select for functional HA variants. Deep sequencing of the variants before and after selection allowed us to infer the H3 site-specific amino-acid preferences. (B) The DMS experiments were completed in biological triplicate, starting from independent preps of the wildtype HA genes to create the mutant plasmids. In addition, we passed and deep sequenced library 3 in technical replicate, denoted 3-1 and 3-2, to estimate the experimental noise within a single biological replicate. (C) Mutation frequencies of nonsynonymous, stop, and synonymous mutations for the mutant DNA, mutant virus, and unmutated DNA and virus controls. There is selection against nonsynonymous and stop codons in the mutant viruses. The percentages signify the frequency of stop codons remaining in the passaged mutant viruses relative to their starting frequency in the mutant plasmid libraries after correcting for the stop codon frequencies in the wildtype DNA and viruses. (D) The Pearson correlations for the amino-acid preferences between each pair of replicates are shown. The correlation between the technical replicates is comparable to that between biological replicates, indicating that the low MOI passage contributes to much of the experimental noise.

existing knowledge about HA's biochemistry. For instance, sites that form structurally important disulfide bridges (sites 52 & 277, 64 & 76, 97 & 139, 281 & 305, 14 & 137-HA2, 144-HA2 & 148-HA2) ([Waterfield et al., 1981](#)) possess high preference for cysteine. At residues involved in receptor binding, there are strong preferences for the amino acids at sites Y98, D190, W153, and S228. A positively charged amino acid at site 329 is important for cleavage activation of the HA0 precursor, and indeed this site exhibits a high preference

Model	ΔAIC	Log Likelihood	Stringency	ω	$\bar{\omega}$	ω_α	ω_β
ExpCM	0.0	-8439.33	2.44	0.91	—	—	—
Goldman-Yang M5	2166.06	-9516.36	—	—	0.36	0.30	0.84
ExpCM, averaged across sites	2504.18	-9691.42	0.68	0.32	—	—	—
Goldman-Yang M0	2607.92	-9738.29	—	0.31	—	—	—

Table 1: The site-specific amino-acid preferences are informative for describing human H3N2 evolution in nature. We implemented several codon substitution models for phylogenetic fitting of an alignment of human H3N2 HA sequences. The maximum likelihood values for each model were compared using the Akaike information criteria (ΔAIC) (Posada and Buckley, 2004). An experimentally-informed codon substitution model (ExpCM) built from the preferences averaged across all replicates performs better than conventional substitution models, specifically the M0 and M5 models in Yang et al. (2000). A non-site-specific ExpCM informed by preferences averaged across all sites performs comparably to the GY94 class of models, indicating the importance of site-specificity in the ExpCM. The optimized parameters for each model are also shown.

for arginine (Kido et al., 1992; Stech et al., 2005). However, a notable exception occurs at the start codon at position -16, which does not show a strong preference for methionine. This codon is part of the signal peptide and is cleaved from the mature HA protein. One possible explanation for why we do not see a strong preference for Met at this site is due to alternative translation initiation occurring at a downstream or upstream start site, as has been described for HA (Girard et al., 2011).

The H3 stalk is relatively mutationally tolerant

We next sought to investigate the inherent mutational tolerance of the Perth/2009 HA. Figure 3 shows the mutational tolerance as calculated from the rescaled Perth/2009 H3 preferences and the rescaled WSN/1933 H1 preferences mapped onto the HA crystal structures. We found antigenic site C and the most distal portion of the globular head near the 190-helix in the Perth/2009 H3 to be tolerant of mutations. Interestingly, the H3 stalk including the shorter α -helix (helix A) is relatively mutationally tolerant compared to the tolerance of the globular head domain. This observation suggests that the stalk may be prone to escape from antibodies, and agrees with previous work demonstrating that it is possible to select for antigenic mutants in H3 by broadly-neutralizing stalk-targeting antibodies (Ekiert et al., 2011; Friesen et al., 2014; Chai et al., 2016; Yamayoshi et al., 2017).

The sites inside the receptor binding pockets are highly functionally constrained and were found to be relatively mutationally intolerant in both H3 and H1 (Wilson et al., 1981). In contrast, the residues surrounding the receptor binding pocket are fairly mutationally tolerant, which may contribute to antigenic evolution as these sites are under strong immune pressure. (Wiley et al., 1981).



Figure 2: The site-specific amino-acid preferences of the Perth/2009 HA. This logplot shows the site-specific amino-acid preferences for the averaged replicates rescaled by the stringency parameter (Table 1) estimated by phydms. The height of each letter is proportional to its preference at that site, and the preferences for all sites are normalized to sum to 1. The sites are in H3 numbering. The top overlay bar shows the relative solvent accessibility. The bottom overlay bar is colored by the HA domain (sig. pep. = signal peptide, HA1 ecto. = HA1 ectodomain, HA2 ecto. = HA2 ectodomain, TM = transmembrane domain, cyto. tail. = cytoplasmic tail). The letters directly above each logo indicate the wildtype amino acid at that site.

The experimental measurements can help discriminate successful influenza virus lineages

A challenge in vaccine strain selection is predicting which strain will dominate the upcoming influenza season. An important question to thereby address is if our experimental measurements are useful in differentiating between strains of human H3N2 influenza virus that have succeeded and those that have died out. To investigate this, we used our preference dataset and an H3N2 phylogeny from 1968-2012 (Figure 4A) to calculate the effects of mutations for the evolutionarily successful trunk lineage and for side branches which have died out. We found that strains with mutations measured to be more beneficial

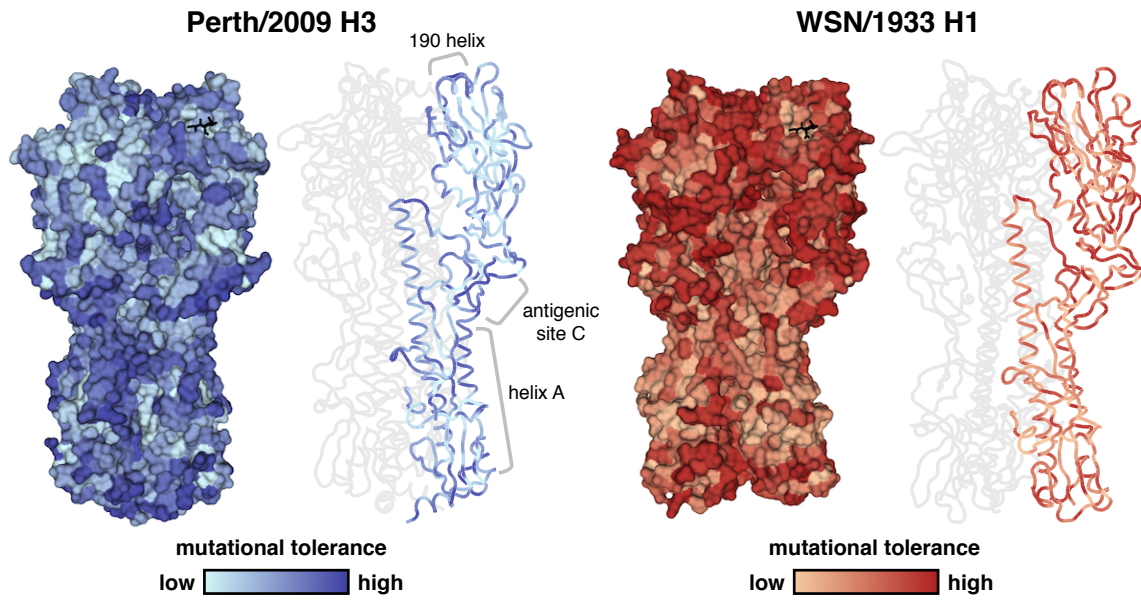


Figure 3: Mutational tolerance mapped onto each site of HA. Mutational tolerance as calculated by the Shannon entropy of a given site's amino-acid preferences are mapped onto the structure of the H3 trimer (PDB 4O5N; Lee et al. (2014)) and the H1 trimer (PDB 1RVX; Gamblin et al. (2004)), with both trimers in approximately the same orientation. The site entropies were calculated from the preferences measured in the Perth/2009 H3 (left panel) from this study, or the preferences measured in the WSN/1933 H1 (right panel) from Doud and Bloom (2016). Lighter shades of blue or red signify low mutational tolerance, while darker shades of blue or red signify high mutational tolerance. For each HA, the structure on the left side colors the full HA trimer, while the structure on the right side colors only one of the monomers. The sialic acid receptor is shown as black sticks. The Perth/2009 H3 shows relatively high mutational tolerance in the stalk region, particularly in helix A, compared to the head region. High mutational tolerance in H3 was also observed near antigenic site C and near the 190 helix. The head region of the WSN/1933 H1 is mutationally tolerant compared to the relatively intolerant stalk region.

to viral growth in our experiments tend to succeed in nature. Figure 4B shows the effects of trunk and side branch mutations in five-year intervals for every year from 1968-2012. On average, trunk mutations are towards more preferred amino acids compared to side branch mutations, and this was true for all intervals. Importantly, trunk mutations are significantly more favorable than side branch mutations when calculating the effects from the entirety of the phylogenetic tree (Figure 4C).

Because tip nodes can contain egg- or cell-passaged isolates (Wu et al., 2017a; McWhite et al., 2016; Skowronski et al., 2016) and our experiments were performed in cell culture, we examined the effects of mutations on terminal side branch nodes to see if these would rank more highly than internal node mutations. Instead, terminal node mutations are on average towards less preferred amino acids than internal node mutations (Figure 4C), and

both internal and terminal node mutations are significantly less favorable than those on the trunk. Therefore, strains that have accumulated mutations that we experimentally measured to be unpreferred generally die out in nature, while more favored mutations provide a selective advantage to the trunk. These findings demonstrate the importance of the functional impacts of HA mutations in determining strain success.

How distantly can the preferences be extended to describe differences in successful and unsuccessful strains? To explore this question, we scored the complete HA sequence of every node in the tree using the preferences by quantifying a *sequence preference* metric. Consistent with the finding that trunk mutations are generally more favorable than side branch mutations, Figure 5 shows that the sequences of trunk nodes also tend to be more highly preferred than those of side branch nodes. Interestingly, the sequence preferences increase over time as the nodes approach the Perth/2009 strain and its closely related nodes, which all exhibit sequence preferences that are higher than that of the trunk. The observation that the strain in which we performed our deep mutational scan has one of the highest sequence preferences illustrates epistatic interactions among mutations such that an unpreferred mutation in one background may be preferred in another.

[*this section will be fleshed out more once I figure out how to plot the substitutions from the root at epitope / non-epitope sites, as per Trevor's suggestion.*] We reasoned that much of the increase in sequence preference toward Perth/2009 could be attributed to epitope sites, as most substitutions have occurred at sites under strong immune pressure. We therefore assessed each node's preference at epitope and non-epitope sites as defined by Wolf et al. (2006). Indeed, the preferences at epitope sites resemble those for all HA sites (Figure 5), with preferences increasing over time. At non-epitope sites, however, the trunk preferences remain relatively constant while side branch preferences tend to drop below the trunk. These observations highlight the extensive epistasis among epitope sites, as has even been noted for sites within the 220-loop surrounding the receptor binding pocket (Wu et al., 2017b). Many successful epitope mutations are likely contingent upon the background in which they arise. Yet, we are able to distinguish trunk sequences as more favorable than side branch sequences, indicating that the preferences are still of utility over short evolutionary timescales.

Can we then distinguish lineage-specific mutational effects using the preferences measured in a distantly related HA homolog? We used the preferences measured previously in the WSN/1933 H1 (Doud and Bloom, 2016) to quantify the effects of H3 trunk and side branch mutations, shown in Figure 6. It is evident that we do not see trunk mutations significantly more favored than side branch mutations, suggesting that our ability to discriminate successful and unsuccessful strains degrades over sufficiently long evolutionary distances.

The H1 and H3 preferences at many sites have shifted

How shifted are the preferences between the distantly related Perth/2009 H3 and WSN/1933 H1 homologs? Although we have previously compared the preferences between related protein homologs of NP ([Doud et al., 2015](#)) and of Env [[cite haddox2017](#)], the HA homologs are considerably more diverged than either of these pairs.

DISCUSSION

We have measured the effect of all possible single amino-acid mutations to Perth/2009 H3 on viral growth in cell culture.

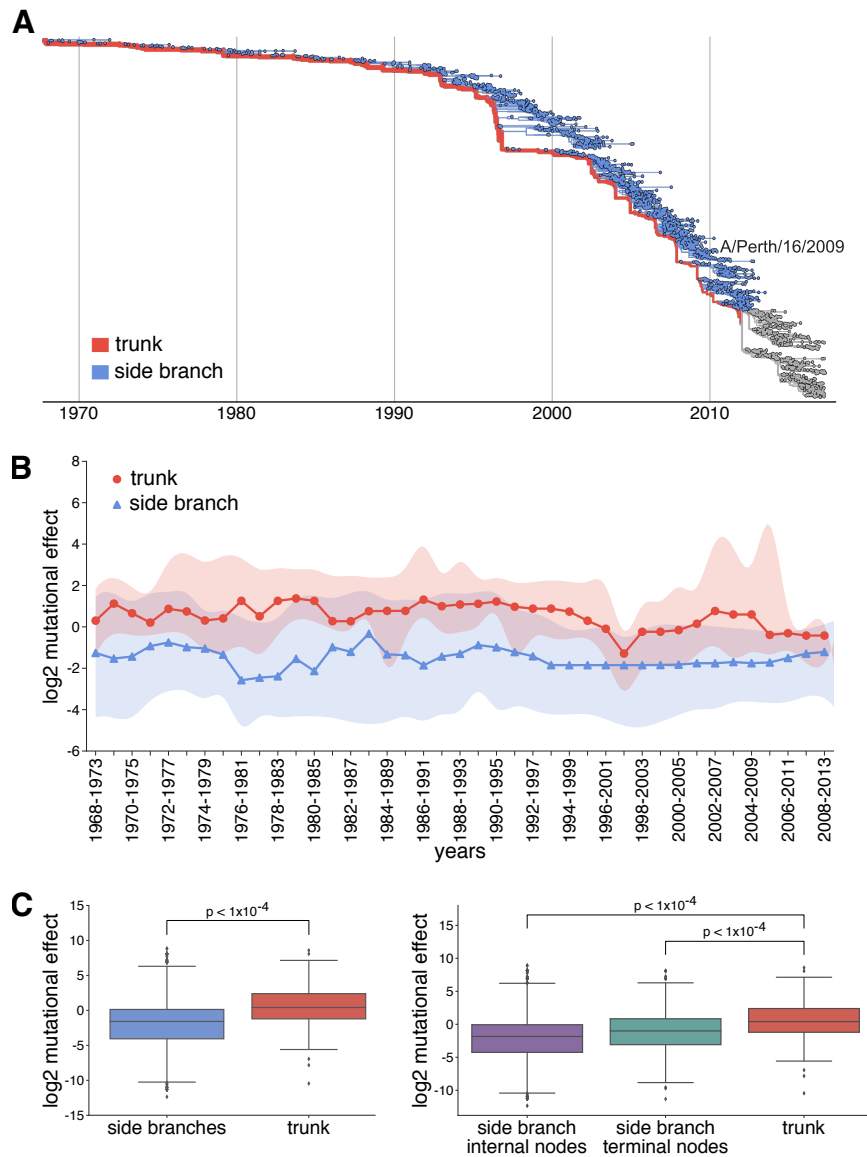


Figure 4: Mutations in evolutionary successful strains tend to be more favorable than in strains that die out. (A) Phylogenetic tree of human H3N2 influenza virus from 1968-present. The trunk is shown in red, and side branches are shown in blue. The gray branches represent the part of the tree for which we cannot yet distinguish the trunk from side branches. (B) Using the Perth/2009 H3 preferences, we calculated the \log_2 mutational effect for trunk and side branch mutations in windows of 5 years for every year from 1968-2013. The median \log_2 mutational effect in a given window is shown as circles for trunk mutations and triangles for side branch mutations. The shaded region demarcates the interquartile range of trunk and side branch mutational effects. Negative numbers signify mutations towards less preferred amino acids, while positive numbers signify more preferred mutations. The median trunk mutational effects are consistently higher than the median side branch mutational effects for all windows. (C) The \log_2 mutational effect for all side branch and all trunk mutations (left panel), in addition to all mutations in internal nodes and terminal nodes on the side branches (right panel) are shown. The preferences were randomized 10,000 times to estimate significance. The effects of trunk mutations are higher than side branch internal and terminal node mutations.

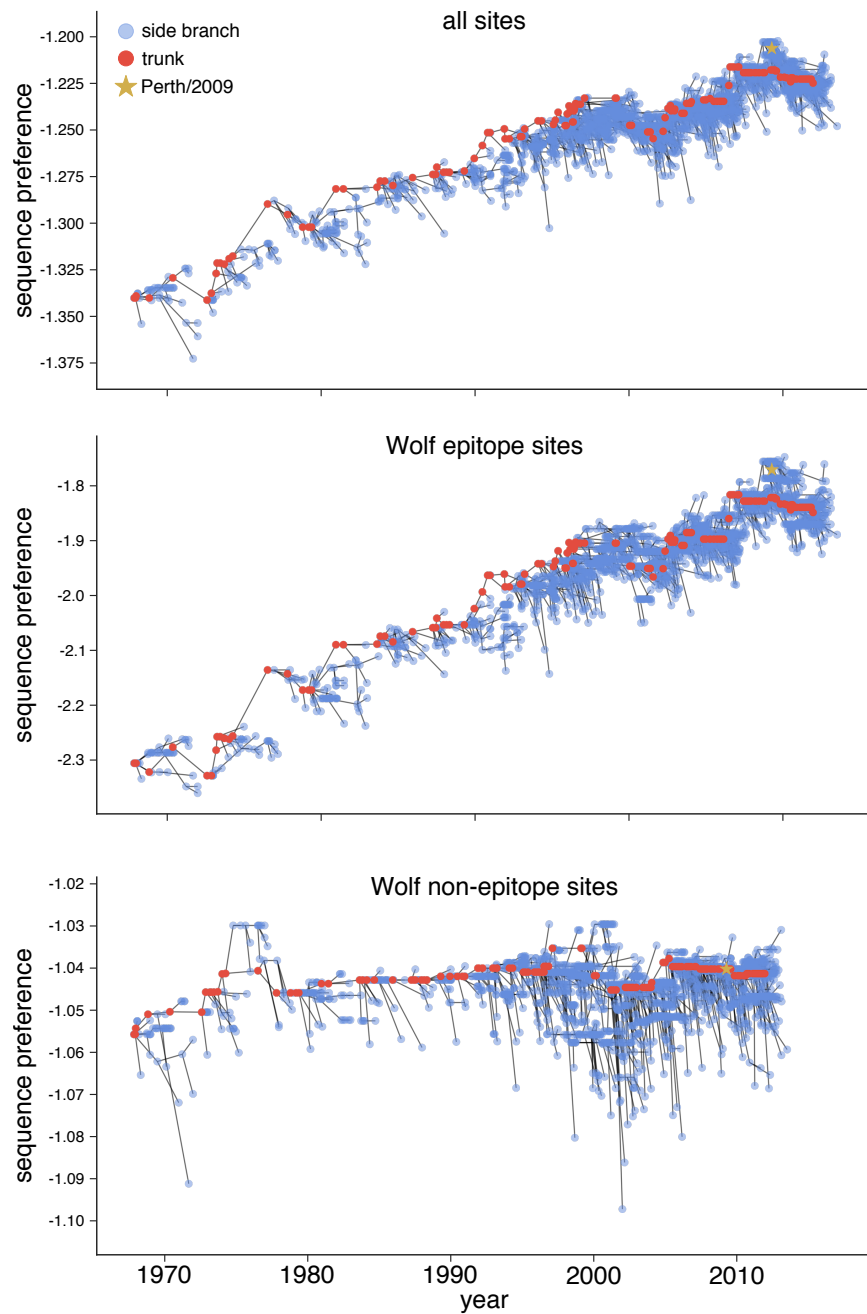


Figure 5: The HA sequences of trunk nodes tend to be more preferred than those of side branch nodes. We used the preferences to calculate the HA sequence preference of every node in a human H3N2 phylogenetic tree. To calculate the sequence preference, we used the entire HA sequence (top panel), only epitope sites (center panel) or non-epitope sites (bottom panel) as defined by [Wolf et al. \(2006\)](#). Higher preferences are closer to zero while lower preferences are more negative. The preferences at all sites and at epitope sites increase as the tree approaches the Perth/2009 strain, indicating epistasis among epitope sites. The trunk nodes generally exhibit higher sequence preferences than do side branch nodes.

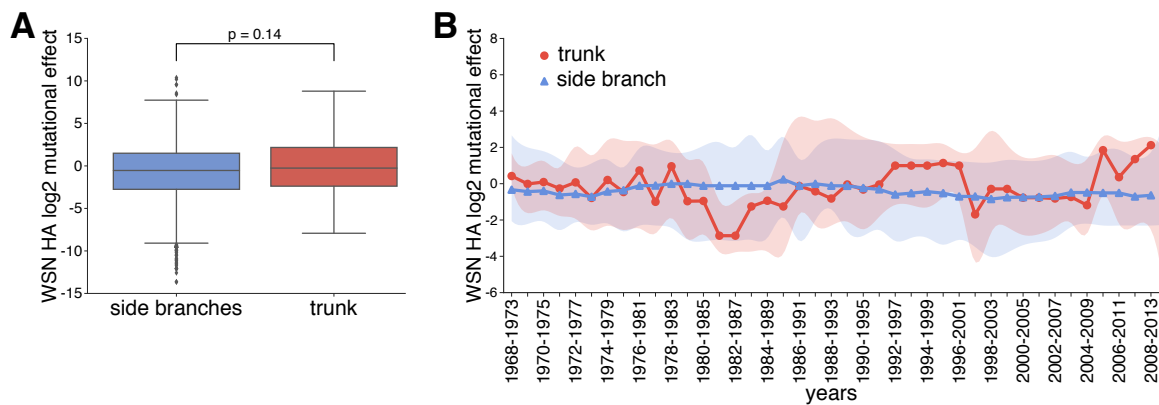


Figure 6: The WSN/1933 H1 preferences do not reveal differences in trunk vs side branch mutational effects (A) We used the WSN/1933 H1 preferences from [Doud and Bloom \(2016\)](#) to calculate the \log_2 mutational effects of trunk and side branch mutations from the inferred H3N2 phylogeny in Figure 4. There is not a significant difference in trunk vs side branch mutational effects. (B) We also performed a sliding window analysis with the WSN/1933 H1 preferences. There is not a distinct difference in trunk and side branch mutational effects.

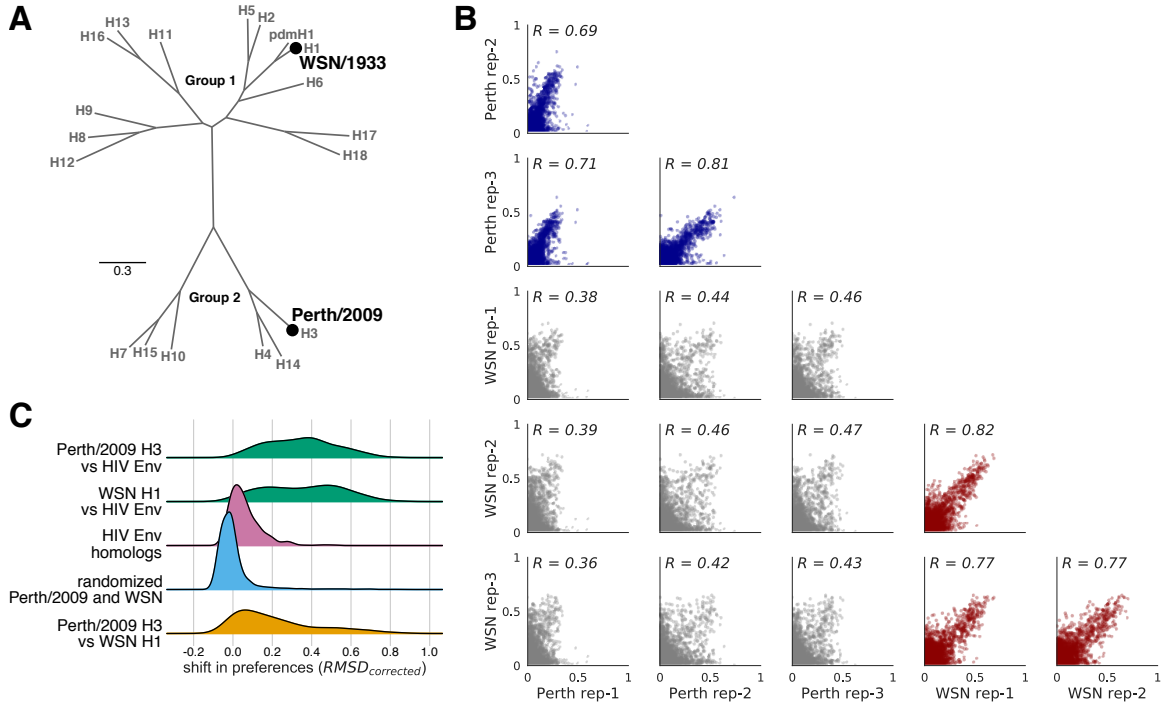


Figure 7: The HA homologs exhibit many large shifts in preference compared to shifts for other viral protein homologs (A) A phylogenetic tree of the HA subtypes, with the two HA's, WSN/1933 H1 and Perth/2009 H3, for which we have measured amino-acid preferences denoted on the tree. The WSN/1933 H1 and the Perth/2009 H3 share $\sim 42\%$ amino-acid identity. (B) The correlations of the amino-acid preferences for replicates both within and between the two HA homologs. The within-Perth/2009 and the within-WSN/1933 correlations are shown in blue and red, respectively. The between homolog correlations are in gray. The correlations for replicates within a homolog are higher than for replicates between homologs. (C) The distribution of shifts in preference for various homolog pairs are shown. The top two distributions show the distances between each of the HA homologs with the non-homologous HIV Env [cite haddox2017]. The center distribution shows the corrected distance between the two HIV Env homologs, which share 86% amino-acid identity. The fourth distribution from the top is a null generated by randomizing the HA replicates and computing the distances. The bottom distribution is the corrected distance between the Perth/2009 H3 and WSN/1933 H1 homologs at all sites that align.

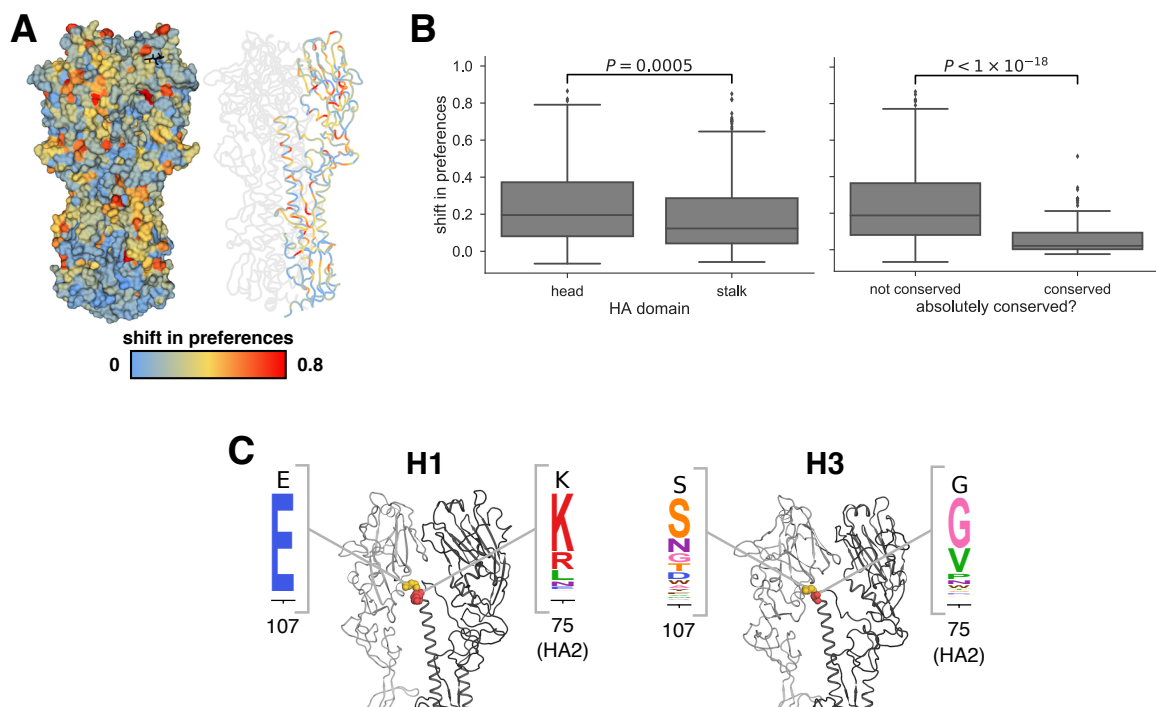


Figure 8: Shifts in preferences mapped onto the structure of HA (A) The preference shifts as calculated by $RMSD_{corrected}$ between the two HA homologs is mapped onto the structure of HA (PDB 4O5N, citation). The left structure shows the HA trimer, and the right structure colors one of the monomers. The sialic acid receptor is shown in black sticks. Gray indicates little shifts in preference, while red indicates large shifts in preference. The top ten most shifted sites are shown in spheres on the monomer. (B)

METHODS

HA numbering

Unless otherwise indicated, all sites are in H3 numbering, with the signal peptide in negative numbers, the HA1 subunit in plain numbers, and the HA2 subunit denoted with "(HA2)". The conversion between sequential numbering of the A/Perth/16/2009 HA and H3 numbering was performed using an HA numbering Python script (available at https://github.com/jbloomlab/HA_numbering).

Creation of MDCK-SIAT1-TMPRSS2 cell line

The human TMPRSS2 cDNA ORF was ordered from OriGene (NM_005656), PCR amplified, and cloned into a pHAGE2 lentiviral vector under an EF1 α -Int promoter and attached to mCherry through an IRES...etc etc [Need to look at Katie's notebooks for this...]

Generation of HA codon mutant plasmid libraries

Recombinant A/Perth/16/2009 (HA, NA) \times A/Puerto Rico/8/1934 influenza virus, NIB-64, NR-41803 was ordered from BEI Resources, NIAID, NIH. Bulk RNA from the viral sample was extracted using the QIAamp Viral RNA Mini Kit (QIAGEN) according to manufacturer's instructions. The Perth/2009 HA and NA genes were then reverse transcribed, PCR amplified, and cloned into the pHW2000 (Hoffmann et al., 2000) and pICR2 [cite?] plasmid backbones.

The codon-mutant libraries were generated using a PCR-based approach described in Dingens et al. (2017).

Generation and passaging of mutant viruses

The mutant virus libraries were generated and passaged using the approach described in Doud and Bloom (2016) with several modifications.

Barcoded subamplicon sequencing

Analysis of deep sequencing data

Inference of phylogenetic trees

[We downloaded X sequences from the Influenza Virus Resource ?.... etc. inferred the tree, ancestral state reconstruction, visualized the tree. Mark Perth/2009 on the tree] To parse out trunk mutations from side branch mutations, we first defined a set of recent nodes sampled on or after Jan. 1, 2017, and traced these nodes back to their most recent common ancestor.

Quantification of mutational effects and sequence preferences from an H3N2 phylogeny

Data availability and source code

Deep sequencing data are available from the Sequence Read Archive under BioSample accessions SAMN08102609 and SAMN08102610. Computer code used to analyze the data and produce the results in the paper are in...

ACKNOWLEDGMENTS

We thank Sarah Hilton, Hugh Haddox, Sidney Bell...the Fred Hutch Genomics Core... Funding...

References

- Bloom JD. 2015. Software for the analysis and visualization of deep mutational scanning data. *BMC Bioinformatics*. 16:1.
- Böttcher E, Matrosovich T, Beyerle M, Klenk H, Garten W, Matrosovich M. 2006. Proteolytic activation of influenza viruses by serine proteases TMPRSS2 and HAT from human airway epithelium. *Journal of Virology*. 80:9896–9898.
- Böttcher-Friebertshäuser, E, Freuer C, Sielaff F, Schmidt S, Eickmann M, Uhlendorff J, Steinmetzer T, Klenk H, Garten W. 2010. Cleavage of influenza virus hemagglutinin by airway proteases TMPRSS2 and HAT differs in subcellular localization and susceptibility to protease inhibitors. *Journal of Virology*. 11:5605–5614.
- Chai N, Swem LR, Reichelt M, et al. (11 co-authors). 2016. Two escape mechanisms of influenza A virus to a broadly neutralizing stalk-binding antibody. *PLoS Pathogens*. 12:e1005702.
- Dingens AS, Haddox HK, Overbaugh J, Bloom JD. 2017. Comprehensive mapping of HIV-1 escape from a broadly neutralizing antibody. *Cell Host & Microbe*. 21:777–787.
- Doud MB, Ashenberg O, Bloom JD. 2015. Site-specific amino acid preferences are mostly conserved in two closely related protein homologs. *Mol. Biol. Evol.* 32:2944–2960.
- Doud MB, Bloom JD. 2016. Accurate measurement of the effects of all amino-acid mutations to influenza hemagglutinin. *Viruses*. 8:155.
- Ekiert DC, Friesen RH, Bhabha G, Kwaks T, Jongeneelen M, Yu W, Ophorst C, Cox F, Korse H, Brandenburg B. 2011. A highly conserved neutralizing epitope on group 2 influenza A viruses. *Science*. 333:843–850.
- Friesen R, Lee P, Stoop E, et al. (23 co-authors). 2014. A common solution to group 2 influenza virus neutralization. *Proc. Natl. Acad. Sci. USA*. 111:445–450.

- Gamblin S, Haire L, Russell R, et al. (11 co-authors). 2004. The structure and receptor binding properties of the 1918 influenza hemagglutinin. *Science*. 303:1838–1842.
- Girard G, Gulyaev A, Olsthoorn R. 2011. Upstream start codon in segment 4 of North American H2 avian influenza A viruses. *Infect. Genet. Evol.* 11:489–495.
- Hilton SK, Doud MB, Bloom JD. 2017. phydms: Software for phylogenetic analyses informed by deep mutational scanning. *PeerJ*. 5:e3657.
- Hoffmann E, Neumann G, Kawaoka Y, Hobom G, Webster RG. 2000. A DNA transfection system for generation of influenza A virus from eight plasmids. *Proc. Natl. Acad. Sci. USA*. 97:6108–6113.
- Kido H, Yokogoshi Y, Sakai K, Tashiro M, Kishino Y, Fukutomi A, Katunuma N. 1992. Isolation and characterization of a novel trypsin-like protease found in rat bronchiolar epithelial Clara cells. A possible activator of the viral fusion glycoprotein. *J Biol Chem*. 267:13573–13579.
- Lee PS, Ohshima N, Stanfield RL, Yu W, Iba Y, Okuno Y, Kurosawa Y, Wilson IA. 2014. Receptor mimicry by antibody F045-092 facilitates universal binding to the H3 subtype of influenza virus. *Nat Commun*. 5:3614.
- McWhite C, Meyer A, Wilke C. 2016. Sequence amplification via cell passaging creates spurious signals of positive adaptation in influenza virus H3N2 hemagglutinin. *Virus Evolution*. 2:vew026.
- Posada D, Buckley TR. 2004. Model selection and model averaging in phylogenetics: advantages of Akaike information criterion and Bayesian approaches over likelihood ratio tests. *Systematic Biology*. 53:793–808.
- Skowronski D, Sabaiduc S, Chamber C, et al. (13 co-authors). 2016. Mutations acquired during cell culture isolation may affect antigenic characterisation of influenza A(H3N2) clade 3C.2a viruses. *Euro Surveill*. 21:30112.
- Stech J, Garn H, Wegmann M, Wagner R, Klenk H. 2005. A new approach to an influenza live vaccine: modification of the cleavage site of hemagglutinin. *Nature Medicine*. 11:683–689.
- Thyagarajan B, Bloom JD. 2014. The inherent mutational tolerance and antigenic evolvability of influenza hemagglutinin. *eLife*. 3:e03300.
- Waterfield M, Scrace G, Skehel J. 1981. Disulphide bonds of haemagglutinin of Asian influenza virus. *Nature*. 289:422–424.
- Wiley D, Wilson I, Skehel J, et al. (4 co-authors). 1981. Structural identification of the antibody-binding sites of hong kong influenza haemagglutinin and their involvement in antigenic variation. *Nature*. 289:373–378.
- Wilson I, Skehel J, Wiley D. 1981. Structure of the haemagglutinin membrane glycoprotein of influenza virus at 3 Å resolution. *Nature*. 289:366–373.

- Wolf Y, Viboud C, Holmes E, Koonin E, Lipman D. 2006. Long intervals of stasis punctuated by bursts of positive selection in the seasonal evolution of influenza A virus. *Biology Direct*. 1:34.
- Wu N, Zost S, Thompson A, Oyen D, Nykolat C, McBride R, Paulson J, Hensley S, Wilson I. 2017a. A structural explanation for the low effectiveness of the seasonal influenza H3N2 vaccine. *PLoS Pathogens*. 13:e1006682.
- Wu NC, Xie J, Zheng T, Nykolat CM, Grande G, Paulson JC, Lerner RA, Wilson IA. 2017b. Diversity of functionally permissive sequences in the receptor-binding site of influenza hemagglutinin. *Cell Host & Microbe*. 21:742–753.
- Yamayoshi S, Ito M, Uraki R, Sasaki T, Ikuta K, Kawaoka Y. 2017. Human protective monoclonal antibodies against the HA stem of group 2 HAs derived from an H3N2 virus-infected human. *Journal of Infection*. .
- Yang Z, Nielsen R, Goldman N, Pedersen AMK. 2000. Codon-substitution models for heterogeneous selection pressure at amino acid sites. *Genetics*. 155:431–449.

Supplementary Material

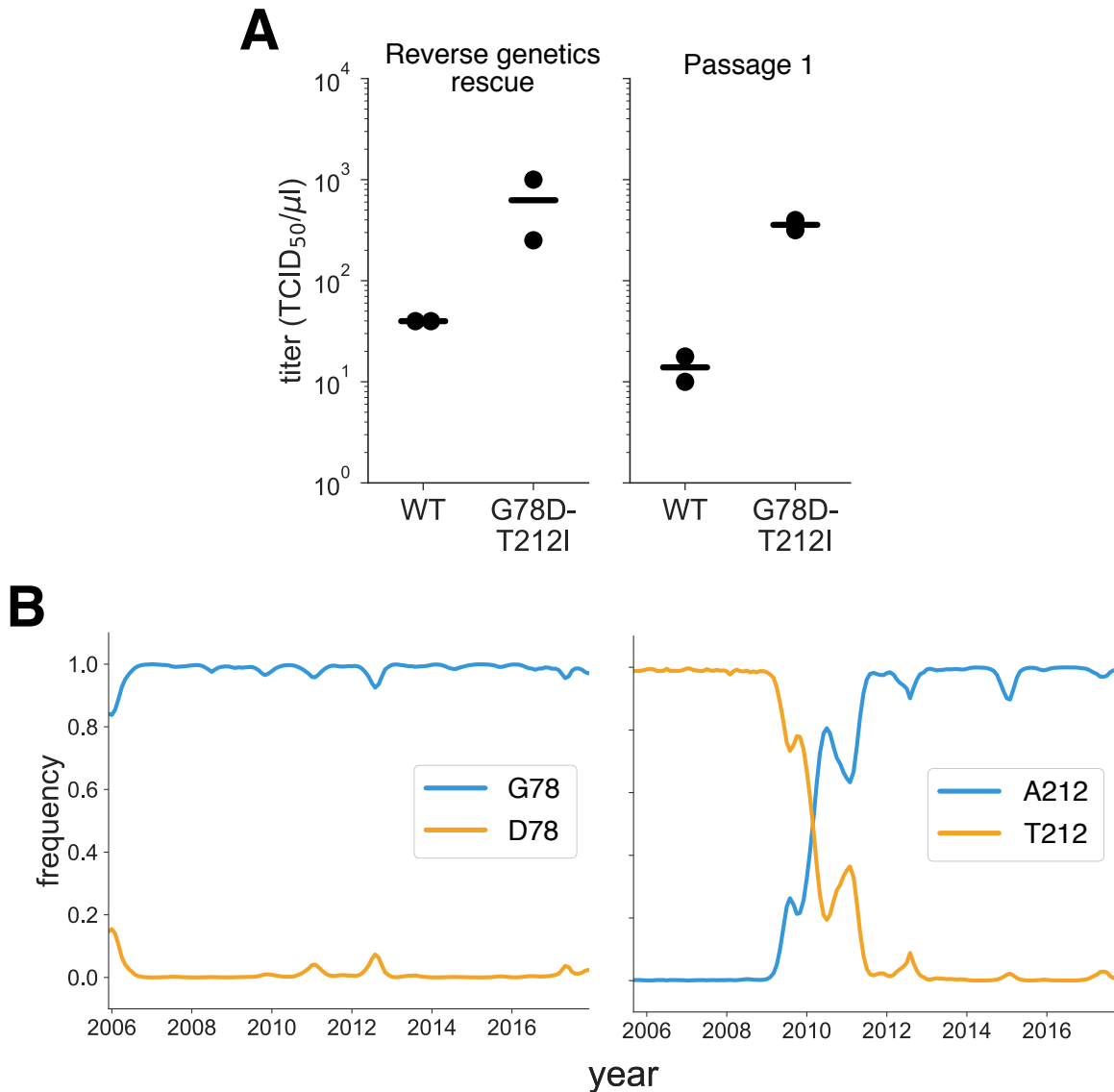


Figure S1: Characterization of the G78D-T212I Perth/2009 HA variant. (A) The G78D-T212I Perth/2009 HA variant grows to higher titers than do viruses carrying the wildtype Perth/2009 HA. Each virus was generated in duplicate by reverse genetics and passaged once at MOI = 0.01 in MDCK-SIAT1-TMPRSS2 cells. The rescue and passage viral supernatants were titered, with the points marking each duplicate and the bar marking the mean. (B) The D78 variant remained at a low frequency in natural human H3N2 sequences over the past ~10 years. The A212 variant rose to fixation in ~2011, replacing the T212 variant.